THE JOURNAL OF PHYSICAL CHEMISTRY B

ARTICLE

pubs.acs.org/JPCB

# Polarity-Sensitive Fluorescent Probes in Lipid Bilayers: Bridging Spectroscopic Behavior and Microenvironment Properties

Giulia Parisio,[†] Alberto Marini,[‡] Alessandro Biancardi,[‡] Alberta Ferrarini,*[,†] and Benedetta Mennucci*[,‡]

[†]Dipartimento di Scienze Chimiche, Università di Padova, via Marzolo 1, 35131 Padova, Italy

[‡]Dipartimento di Chimica e Chimica Industriale, Università di Pisa, via Risorgimento 35, 56126 Pisa, Italy

Supporting Information

**ABSTRACT:** We have studied the emission features of the fluorescent polarity-sensitive probes known as Prodan and Laurdan in a liquid-crystalline DPPC bilayer. To this purpose, we have combined high-level quantum mechanical electronic structure calculations with a molecular field theory for the positional−orientational−conformational distribution of the probes, in their ground and excited states, inside of the lipid bilayer, taking into account at both levels the nonuniformity and anisotropy of the environment. Thus, we can interpret the features of the fluorescence spectra of Prodan and Laurdan in relation to the position and orientation of their chromophore in the bilayer. We have found that the environment polarity is not sufficient to explain the large red shifts experimentally observed and that specific effects due to hydrogen bonding must be considered. We show that the orientation of the probe is important in determining the accessibility to water of the H-bond-acceptor group; in the case of Laurdan interesting conformational effects are highlighted.

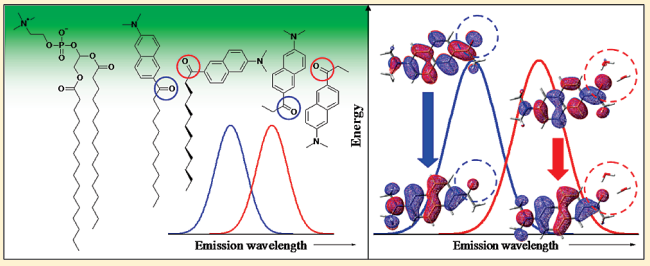


## 1. INTRODUCTION

Polarity-sensitive fluorescence probes bear chromophores that exhibit a change of their emission characteristics as a function of the local polarity of their surroundings. This makes them extremely useful to investigate the structural and dynamical properties of biological and model membranes. Despite their wide use, a precise understanding of the connection between spectroscopic response and probe−membrane interaction is still lacking, and the interpretation of experimental results presents controversial issues. The 6-acyl-2-(*N*,*N*-dimethylamino)naphthalene derivatives known as Prodan (propionyl) and Laurdan (lauroyl) are important examples in this field.[1−6] Their molecular structures, together with that of the shorter tail homologue Acdan, 6-acetyl-2-(*N*,*N*-dimethylamino)naphthalene, are shown in Figure 1. The presence of an electron-donor dimethylamino group and an electron-accepting carbonyl group, on opposite sides of the naphthalene core, gives these fluorophores an intramolecular charge-transfer (ICT) character.[7] In isotropic solvents, they exhibit a fluorescence emission that changes with the polarity of the environment; it shifts from ∼430 to ∼530 nm upon going from cyclohexane to water.[8−10] A distinction can be made between protic and nonprotic solvents; whereas in the latter case the spectral effects can be explained by a generic mechanism of solvent reorganization, with Stokes shifts that scale with the dielectric permittivity of the solvent, a major role of hydrogen bonding has been invoked for the dramatic emission effects observed in protic solvents.[11,12]

The fluorescence spectra of 6-acyl-2-(*N*,*N*-dimethylamino)-naphthalene dyes in lipid bilayers exhibit two bands, centered at ∼440 and ∼490 nm.[1,13−15] In some cases, additional emission at about 520 nm was found, which was ascribed to dye partitioning in water.[16] Remarkable variations were observed upon going from the liquid-crystalline to the gel phase, as well as under changes of membrane composition; therefore, these probes were devised as suitable to monitor phase transitions and to assess the lateral heterogeneity of lipid bilayers.[6] Moreover, they were proposed as reporters of changes in membrane organization induced by pressure,[1,17] curvature,[18] and strains,[19] as well as by addition of cholesterol,[13,20,21] local anesthetics, and alcohols.[1,16,21,22]

Different explanations were proposed for the spectral features of the fluorescence emission and, in general, for the results of fluorescence experiments in membranes; after many studies, however, there remain controversial issues. The red shift is generally believed to reflect changes in the polarity of the microenvironment related to the amount of water accessible to the probe,[13] and a crucial role of the mobility of water and/or lipids was stressed.[1,22−26] It was discussed whether the change of polarity should be taken as an indication of lateral heterogeneity (due to the presence of domains differing in physical state and composition)[13] or could rather reflect the location of the probe at different depths.[1] From the influence of the chemical structure of phospholipid head groups and from the absence of very fast contributions (on the picosecond time scale) to solvent relaxation, some authors inferred that water molecules should not

**Received:** June 1, 2011
**Revised:** July 14, 2011
**Published:** July 19, 2011





dx.doi.org/10.1021/jp205163w | *J. Phys. Chem. B* 2011, 115, 9980–9989

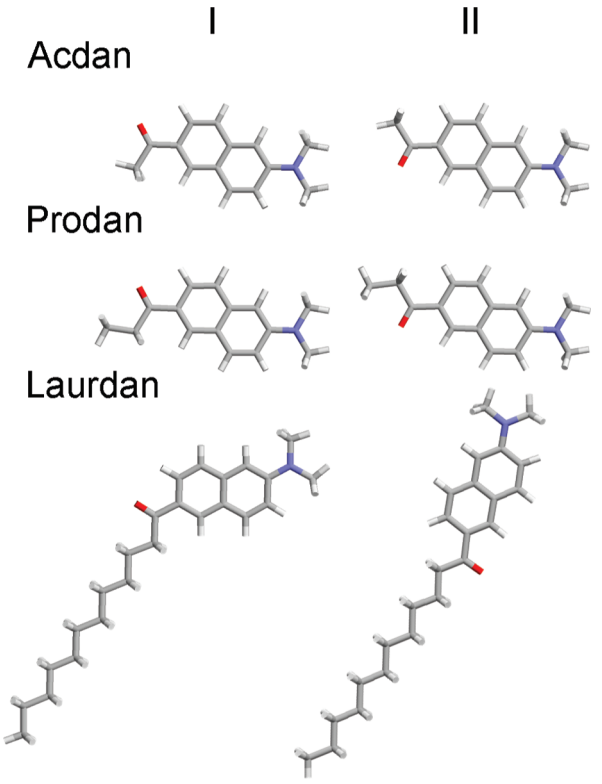


**Figure 1.** Molecular structures of the fluorescent probes Acdan, Prodan, and Laurdan. For each probe, two conformers are shown, differing for the orientation of carbonyl oxygen, which points either toward the $\beta$ (I) or the $\alpha$ (II) naphthalene position. Acyl chains in the all- trans chain conformation are shown.

be intended as free but rather as bound to the lipid head groups.[5,27−29] Another issue concerns hydrogen bonding;[22,30,31] it has been argued that a generic dipolar effect is not sufficient to produce fluorescence shifts as large as those observed in experiments, and the presence of two forms of the probe, H-bonded and non-H-bonded, has been hypothesized, the former of which would be responsible for the emission at about 490 nm.

Despite the presence of the same chromophore, differences in the behavior of Prodan and Laurdan were evidenced by fluorescence[32] and FTIR studies.[16,33] These were generally ascribed to the different positions of the two probes. For Prodan a heterogeneous distribution was proposed,[28] as well as a relocation between regions more or less rich in water upon changes in the bilayer organization, caused by phase transition.[1,16,32,33]

There is also uncertainty on the nature of the emissive states. In particular, a long-term controversy is whether Prodan fluorescence occurs from a planar or from a twisted state. Abelt and co-workers[34] investigated the photophysical properties of several Prodan derivatives, where the dialkylamino group is constrained to be planar or perpendicular with respect to the naphthalene ring, by means of experimental solvatochromism studies. They found that constrained planar analogues behave just like Prodan, while twisted analogues behave very differently, and in addition, they have a pyramidal, rather than a planar, amino group. All of this considered, they concluded that Prodan emission is from a planar ICT state. Several quantum mechanical (QM) studies have been also carried out to characterize the electronic states of Prodan, its structure, and spectroscopic behavior in various solvents.[11,12,35,36] The most recent studies, in which accurate QM approaches are used, seem to unequivocally show that a twisted excited state is not necessary to explain both the large Stokes shifts and the large solvatochromism that characterize Prodan (and its analogues) but that a planar excited state involving a significant rearrangement of the electronic density properly describes all of the specific spectroscopic signatures. In particular, a recent study of some of the present authors[12] has shown that this description is still valid in protic solvents. In fact, strongly interacting excited solute−solvent clusters are formed due to specific effects of H-bonding nature, which, when combined to longer-range solvent effects, are responsible for the significant red shift found in the fluorescence of Prodan moving from a polar but aprotic solvent to a protic one. A previous computational study also explored the combined role of H-bonding effects and a nonuniform dielectric environment on the dependence of the absorption and emission energies of Prodan on its position and orientation across a diffuse interface.[36] However, the lack of information on the probe distribution in membranes precluded direct connection with experimental observables.

Here, we propose an integrated computational methodology, complementing a QM description of electronic transitions based on the extension of the polarizable continuum model (PCM)[37] to interfaces[38] with a recent molecular field theory (MFT) for the free energy of the probe in the lipid bilayer.[39] At both levels, a consistent model of the bilayer is used, treated as a nonuniform and anisotropic continuum. Alternatively, atomistic molecular dynamics simulations could be used;[57] these provide insight into the structure and dynamics of the solvent, but very long and computationally demanding trajectories are needed to achieve a statistically meaningful sampling of the wide space of configurations accessible to the probes. The computational cost is dramatically reduced by the MFT membrane model, where the molecularity of the solvent is lost, but with the advantage of a clear connection between the properties of the environment and their effects. Specific aspects of solute−solvent interactions, if needed, may also be introduced into this picture in a suitable way. Here, we apply our integrated methodology to Acdan, Prodan, and Laurdan in a liquid-crystalline dipalmitoylphosphatidylcholine (DPPC) bilayer; theoretical predictions are compared with literature experimental data in order to explain the observed spectroscopic signatures of these probes.

## 2. METHODS

Nonuniformity and anisotropy are major characteristics of lipid bilayers that strongly influence their interaction with molecular probes. The dielectric constant jumps from about 80 in water to a value close to 2 in the bilayer interior.[40] As a consequence of the constraints imposed by the interface, the density and the order of acyl chains exhibit gradients across the bilayer.[41] Impressive effects are evidenced by the lateral pressure profile, which exhibits changes of hundreds of bars within a few Ångström.[42] A distinctive feature of the approach proposed in this work is the integration of theoretical models, recently developed in different contexts by the present authors, which take into account the heterogeneity and anisotropy of the environment within a continuum bilayer representation. To describe the distribution of solutes, the position and orientation dependence of short-range repulsive, dispersion, and electrostatic interactions is considered;[39] the direct effect of the latter on the electronic

distribution of the probe is included in calculations of electronic states and transitions.[36]

**2.1. QM/PCM Approach for Interfaces.** The PCM[37] belongs to the family of solvation models in which the solvent is described as a structureless continuum, characterized by its dielectric permittivity, $\varepsilon$. Within this framework, a (molecular) well-shaped empty cavity is built to house the solute, which is fully described by its charge distribution $\rho$. The resulting electrostatic problem for the solute−solvent system is solved by introducing an apparent surface charge, $\sigma$, on the cavity surface that represents the polarization of the medium. In turn, $\sigma$ gives rise to a solvent reaction field (expressed in terms of the corresponding potential) acting back on the solute. In the present study, the integral equation formalism (IEF)[43] version of PCM has been used; this version allows application of exactly the same strategy to very different media ranging from standard isotropic solvents characterized by a scalar permittivity to anisotropic dielectrics like liquid crystals and polymers, passing through interfaces, as we shall show in the following.

When a QM description of the solute charge density $\rho$ is used, the basic idea is to define an "effective" solute Hamiltonian as a sum of two terms; one refers to the solute in the empty space and the other describes the solute−solvent interaction. As in the computational practice, a boundary-element method is introduced by partitioning the cavity surface into finite elements, the apparent charge $\sigma$ is substituted by point charges $q(\mathbf{s}_k)$, placed at the center $(\mathbf{s}_k)$ of each element, and the solute−solvent interaction term is written as

$$\hat{V}^{\mathrm{IEF}}(\mathbf{r}) = \sum_k \frac{1}{|\mathbf{r} - \mathbf{s}_k|} q(\mathbf{s}_k; \varepsilon, \rho) \tag{1}$$

where $\mathbf{r}$ is the electronic coordinate, and we have reported the explicit indication of the dependence of the apparent charges $q$ on the solvent dielectric constant $\varepsilon$ and the solute charge density $\rho$.

The nature of the system under study enters $\hat{V}^{\mathrm{IEF}}$ via the values of the apparent charges that depend on the specific characteristics (isotropy, homogeneity, etc.) of the environment. The theoretical apparatus needed to compute $q(\mathbf{s}_k;\varepsilon,\rho)$ in the presence of inhomogeneous media, such as liquid/liquid interfaces, liquid/gas interfaces, or planar membranes, within PCM has been discussed in detail in ref 38. In particular, all of these inhomogeneous systems can be treated by modeling the environment as a dielectric medium characterized by a permittivity continuously varying along the normal to the interface. Due to the flexibility of the PCM procedure, any continuous profile for the permittivity, with a not too large derivative and that does not cross the zero, can be considered.

The procedure outlined above is not limited to calculations on the ground-state density of the molecule, but it can be used for excited states as well. Here, in particular, we adopt the PCM extension to the time-dependent density functional theory (TDDFT). In these calculations, in addition to the static permittivity profile, we also need to know the dynamic equivalent. However, as the changes of the latter are extremely small (going from 2 for the apolar part of the bilayer to 1.78 for water), we have considered a position-independent average value. The same TDDFT approach coupled to PCM can be further extended to obtain derivatives of the transition energies[44] and applied to geometry optimization of excited states. It is thus possible to calculate emission energies of relaxed excited states taking into account the effect of the environment in all steps of the calculations.

**2.2. Molecular Field Theory (MFT) for Solutes in Lipid Bilayers.** A lipid bilayer in the liquid-crystal phase is a uniaxial environment, where the symmetry axis is parallel to the bilayer normal. Our description of the positional and orientational distribution of a molecular solute in this environment is based on the definition of a molecular field potential, $U$, which is expressed as the superposition of four contributions; these are associated with the work required to form a molecular-shaped cavity ($U_{\mathrm{cav}}$), with the electrostatic ($U_{\mathrm{el}}$) and dispersion ($U_{\mathrm{disp}}$) solute−bilayer interactions, and with the anisotropic interactions between the solute and the ordered acyl chains in the membrane interior ($U_{\mathrm{ord}}$)[39]

$$U = U_{\mathrm{cav}} + U_{\mathrm{el}} + U_{\mathrm{disp}} + U_{\mathrm{ord}} \tag{2}$$

Due to the nonuniform and anisotropic nature of the bilayer environment, each term in eq 2 bears a dependence on the position of the solute along the bilayer normal, $Z$, and on its orientation with respect to the normal, $\Omega$. The profile of the lateral pressure opposing the formation of the molecular cavity, whose high nonuniformity originates from the modulation of lipid−lipid repulsions and attractions across the bilayer, enters the first term in eq 2.[49] The gradients of density and dielectric permittivity along the normal affect the dispersion and the electrostatic term, respectively, the former described by a generalized London expression[50] and the latter by a generalized Born model.[51] The order parameter profile, describing the average alignment of acyl chain bonds to the bilayer normal, is used to parametrize the anisotropic interactions in the last term in eq 2, within a theoretical model originally proposed for liquid crystals.[52] An atomistic representation of the solute is used, in terms of its atomic charges and polarizabilities and of the solvent excluded molecular surface. In the case of flexible solutes, the mean-field potential defined in this way also depends on the molecular conformation, specified by the torsional angles $\chi$.

The mean-field potential $U(Z,\Omega,\chi)$ is related to the coupled positional−orientational−conformational distribution function $P(Z,\Omega,\chi)$ by $P(Z,\Omega,\chi) = \exp[-U(Z,\Omega,\chi)/k_{\mathrm{B}}T]/Q$, with the partition function $Q = \int \mathrm{d}Z \int \mathrm{d}\Omega \int \mathrm{d}\chi \exp[-U(Z,\Omega,\chi)/k_{\mathrm{B}}T]$. By properly averaging $P(Z,\Omega,\chi)$ over the orientational and conformational variables, the reduced position distribution function $P_{\Omega,\chi}(Z)$ is defined, such that $P_{\Omega,\chi}(Z)\,\mathrm{d}Z$ gives the probability that the solute is located in the element $\mathrm{d}Z$ centered at the $Z$ position, irrespective of its orientation and conformation. We can also define a position-dependent free energy, $u_{\Omega,\chi}(Z) = \mathrm{const} - k_{\mathrm{B}}T \ln P_{\Omega,\chi}(Z)$, which can be interpreted as the transfer free energy from bulk water to the $Z$ position in the bilayer, if $\mathrm{const} = k_{\mathrm{B}}T \ln P_{\chi}^{\mathrm{bw}}$, where $P_{\chi}^{\mathrm{bw}}$ is the reduced distribution in bulk water.

**2.3. Computational Details.** *Electronic States and Transitions of the Probes.* Geometries for the probes in their ground state $S_0$ and in the first excited state $S_1$, in vacuum and in solution, were determined by means of the (TD)DFT method using the CAM-B3LYP functional[45] and the 6-311+G(d,p) basis set. The choice of the CAM-B3LYP functional has been dictated by the results obtained in previous studies,[12,36] which have shown that standard hybrid functionals fail at describing the real structure of the emitting state of Prodan. By contrast, CAM-B3LYP, which has been developed to improve DFT performances in treating long-range exchange interactions, correctly reproduces the structures and the energetics obtained with highly correlated ab initio methods. PCM has been used to describe the effects of the

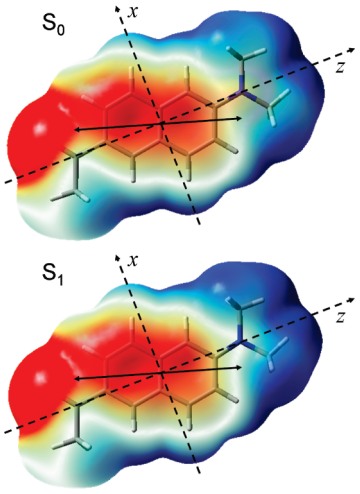


**Figure 2.** Molecular structure of the I conformer of Acdan in the ground $S_0$ (top) and excited $S_1$ (bottom) states. The electrostatic potential is mapped on an isodensity surface (negative to positive from red to blue). Superimposed on each structure we show the molecular reference frames (dashed lines) and the transition dipole moments (solid arrows).

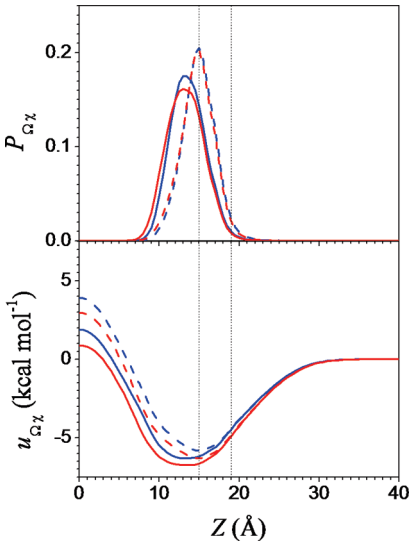


**Figure 3.** Transfer free energy $u_{\Omega,\chi}(Z)$ (bottom) and position distribution function $P_{\Omega,\chi}(Z)$ (top) calculated for Acdan (blue line) and Prodan (red line) in the $S_0$ (solid line) and $S_1$ (dashed line) states as a function of the position of the center of the molecular frame across the lipid bilayer. The coordinate $Z = 0$ corresponds to the bilayer midplane; the vertical lines indicate the average position of the carbonyl and phosphate groups of lipid molecules. Given the symmetry of the system, only one-half of the bilayer is shown.

environment, with molecular cavities built as a series of interlocking spheres centered on atoms, as in ref 36.

Atomic charges (ESP charges) in the $S_0$ and $S_1$ states have been calculated at the same level, according to the Merz–Singh–Kollman scheme[47] applied to ground- and excited-state geometries and the electronic density in vacuum, respectively.

Figure 2 shows the molecular structure of conformer I of Acdan, with the molecular reference frame taken for the probes superimposed (the molecular frame of the II conformer is defined in the same way, with the $x$ axis pointing in the direction of the carbonyl oxygen). The electrostatic potentials for the molecule in the $S_0$ and in the $S_1$ states, and the corresponding transition dipole moments, all calculated in vacuum, are also reported in Figure 2.

PCM vertical absorption and emission energies were obtained by exploiting the corrected linear response scheme.[46] The analysis of fluorescence emission energies in the membrane environment was performed for the Acdan due to their negligible dependence on the length of the acyl chain and for obvious computational reasons. The results that we shall present refer to the probe in conformation I, but we checked, on selected points, that results for the other conformation were not significantly different. The molecular geometry of Acdan in its first singlet excited state was optimized in bulk water and was kept fixed for all subsequent calculations.

*Probe Representation in the MFT Model.* The atomistic representation of the probes encompasses their three-dimensional structure and the solvent excluded molecular surface,[48] in addition to their atomic charges and polarizabilities. Optimized geometries and atomic ESP charges in vacuum were used as obtained from the QM calculations described above. Molecular surface and atomic polarizability were parametrized as described in ref 39. Calculations were performed for the probes in their ground ($S_0$) and excited ($S_1$) states.

The probe flexibility was introduced in terms of conformers, each corresponding to a local minimum of the torsional potential.[53] Two equivalent states were taken for the $C_{ar}$–CO bond, both with the R–C=O group in the plane of the naphthalene rings but the C=O bond on either the side of the $\beta$ (conformer I) or that of the $\alpha$ carbon (conformer II) of the adjacent ring (see Figure 1). In the case of Laurdan, also the flexibility of the acyl chain was taken into account. For the acyl chain bonds, the three states usually denoted as trans, gauche$_+$, and gauche$_-$ were considered. The all- trans conformers, shown in Figure 1, are the most stable in vacuum; the energy increases upon introduction of a gauche state in the C(O)–$CH_2$ and $CH_2$–$CH_2$ bonds (by 0.13 and 0.51 kcal mol$^{-1}$, respectively, from calculations at the MP2/6-31G(d,p) level). For simplicity, only conformers with a single gauche state in the acyl chain were included in our analysis; thus, a total number of 42 conformers was obtained.

*Bilayer Representation.* Lateral pressure,[54] mass density[55] and $S_{CD}$ order parameter[56] profiles, used for the molecular field calculations, were taken from molecular dynamics simulations of a DPPC bilayer in the liquid-crystal phase at the temperature $T = 323$ K. A consistent set of these profiles was available from the literature because DPPC is one of the most widely investigated lipid systems. The same dielectric constant profile was assumed for the molecular field and the QM/PCM calculations; it was evaluated on the basis of a three-dielectric model, as proposed in ref 51.

## 3. RESULTS

**3.1. Free-Energy Profiles and Distributions.** Figure 3 shows the water/bilayer transfer free-energy profile $u_{\Omega,\chi}(Z)$ and the corresponding position distribution function $P_{\Omega,\chi}(Z)$ calculated for Acdan and Prodan in the $S_0$ and $S_1$ states, with $Z$ being the position along the bilayer normal of the origin of the molecular frame, defined as in Figure 2. Practically identical results were obtained for conformers I and II of the probes.


dx.doi.org/10.1021/jp205163w |J. Phys. Chem. B 2011, 115, 9980–9989

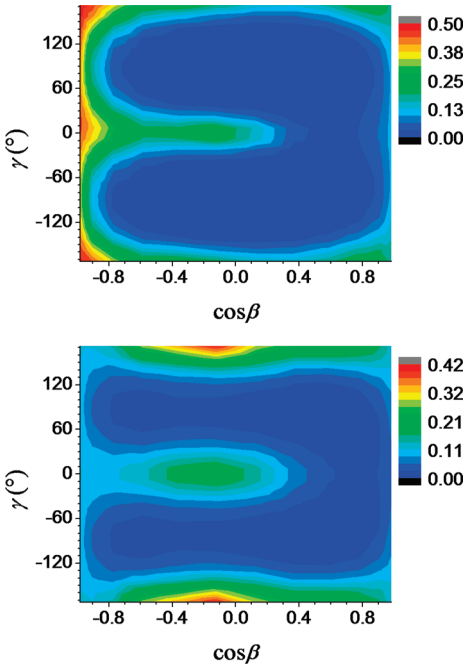


**Figure 4.** Orientational probability distribution calculated for conformer I of Prodan in the $S_0$ (top) and $S_1$ (bottom) states, at distances of 13.5 and 15.0 Å from the bilayer midplane, respectively. $\beta$ is the angle between the bilayer normal and the molecular $z$ axis, and $\gamma$ defines a rotation around this axis (for $\gamma$ = 0 and 180°, the naphthyl plane is perpendicular to the bilayer surface).

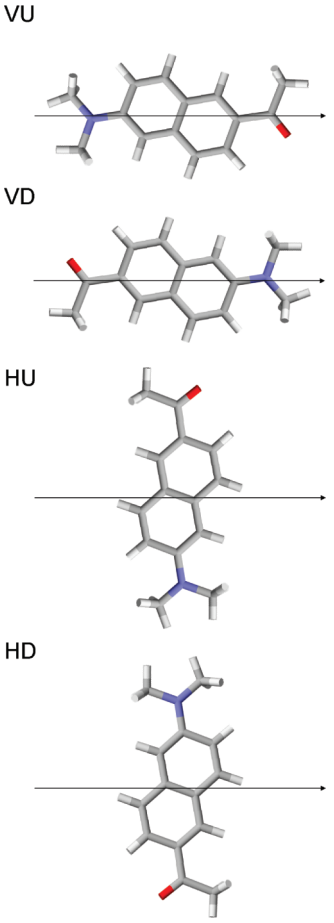


**Figure 5.** Orientations of the chromophore with respect to the normal to the bilayer, selected on the basis of our analysis of the orientational distribution in the lipid bilayer (shown for Acdan). Arrows indicate the bilayer normal (pointing toward water).

The free-energy profiles exhibit a well about 6−7 kcal mol$^{-1}$ deep in the region between 10 and 19 Å from the bilayer midplane, slightly lower for Prodan than for Acdan, with some difference between the ground and the excited states. The corresponding position distribution profiles indicate a preference of the two probes for locating the center of their naphthalene moiety near the hydrophobic/hydrophilic interface, which is generally identified with the region where the carbonyl groups of lipids reside; vanishing probability in the central region of the bilayer is predicted. The excited-state distributions are a little narrower than those in the ground state, and their maximum is slightly shifted toward the polar region, which can be traced back to electrostatic effects. In fact, in agreement with experiment,[30] an increase of the molecular dipole moment, from about 6 to about 10 D, is predicted upon going from the ground to the excited state. As shown in Figure 2, this corresponds to an enhancement of the exposed charges on the electron-donor and -acceptor groups in the chromophore.

The analysis of the different contributions to the mean-field potential, eq 2, shows that dispersion interactions are the main determinants of the partitioning of Acdan and Prodan in the bilayer; in their absence, the free-energy profile would be nearly flat and would only exhibit an appreciable increase for insertion of the probes deep in the bilayer core due to the energetic cost associated with charges buried in the apolar region. Electrostatic interactions are relatively weak but have a peculiar effect by stabilizing positions and orientations that allow the exposed charges, which are mainly located in the carbonyl and in the amino groups, to reside close to water. The location of the probes close to the hydrophilic/hydrophobic interface is also promoted by a drop in the lateral pressure of the bilayer,[42] which favors the formation of a molecular cavity in this region. Anisotropic interactions with the acyl chains stabilize orientations of the long molecular axis nearly parallel to the bilayer normal and insertion in the most ordered region, with the result of slightly broadening the position distribution of the probes.

Figure 4 shows the orientational probability distribution calculated for the conformer I of Prodan in its preferred position in the $S_0$ and $S_1$ states. The plots show a strong anisotropy, with a pronounced tendency of the molecule to keep the naphthalene plane perpendicular to the bilayer surface. The probe in the ground state preferentially aligns its long axis parallel to the bilayer normal, with the carbonyl or, to a lesser extent, the dimethylamino group pointing toward water. In the $S_1$ state, the perpendicular orientation is stabilized over the parallel, with the carbonyl either pointing toward water or, with a lower probability, toward the bilayer core. This can be ascribed to the increased charges on exposed atoms because the horizontal alignment allows the molecule, as a whole, to reside in a more polar environment. The orientational distribution of Acdan exhibits analogous features, except for an even more pronounced preference for directing the C═O group toward water due to the weaker hydrophobic character of its acyl end.

We collect in Figure 5 the preferred orientations of the chromophore, represented for Acdan, as obtained from the


dx.doi.org/10.1021/jp205163w |J. Phys. Chem. B 2011, 115, 9980–9989

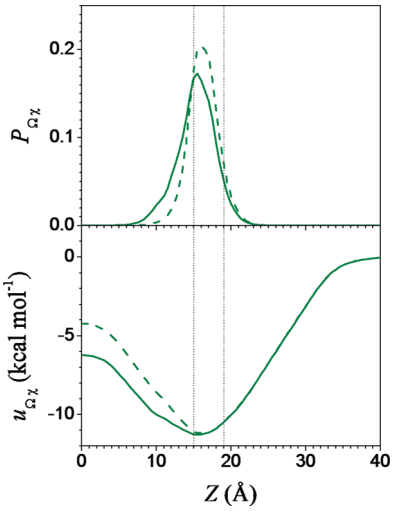


**Figure 6.** Transfer free energy $u_{\Omega,\chi}(Z)$ (bottom) and position distribution function $P_{\Omega,\chi}(Z)$ (top) calculated for Laurdan in the $S_0$ (solid line) and $S_1$ (dashed line) states as a function of the position of the center of the molecular frame across the lipid bilayer. The coordinate $Z = 0$ corresponds to the bilayer midplane; the vertical lines indicate the average positions of the carbonyl and phosphate groups of lipid molecules. Given the symmetry of the system, only one-half of the bilayer is shown.

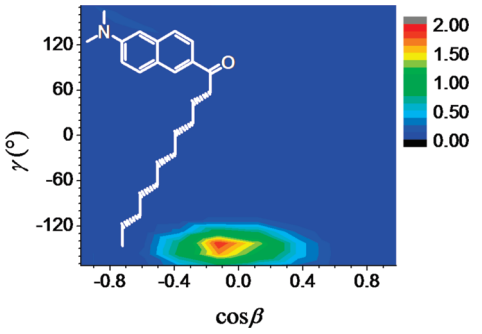


**Figure 7.** Orientational probability distribution calculated for an L-shaped conformer of Laurdan in the $S_0$ state at $Z = 15.5$ Å. $\beta$ is the angle between the bilayer normal and the molecular $z$ axis, and $\gamma$ defines a rotation around this axis (for $\gamma = 0$ and 180°, the naphthyl plane is perpendicular to the bilayer surface).

analysis just discussed. These orientations will be henceforth denoted as **VU** (vertical, C═O up, $\cos\beta = -1$), **VD** (vertical, C═O down, $\cos\beta = 1$), **HU** (horizontal, C═O up, $\cos\beta = 0$ and $\gamma = 180°$), and **HD** (horizontal, C═O down, $\cos\beta = 0$ and $\gamma = 0°$).

In the case of Laurdan, the long acyl chain significantly affects the interaction with the lipid bilayer. Figure 6 shows the transfer free-energy profile $u_{\Omega,\chi}(Z)$ and the probability distribution $P_{\Omega,\chi}(Z)$ in the $S_0$ and $S_1$ states, calculated by averaging over all conformers. A free energy well about 11 kcal mol$^{-1}$ deep is predicted, the lauroyl tail being responsible for the greater affinity of this probe for the membrane environment in comparison to the shorter-chain homologues. The distribution of the chromophore moiety reaches its maximum at the hydrophobic/hydrophilic interface and is broadened by the contribution of different conformers. A distinction between L-shaped (like I in Figure 1) and elongated conformers (like II in Figure 1) emerges from the conformational analysis, the former being generally stabilized

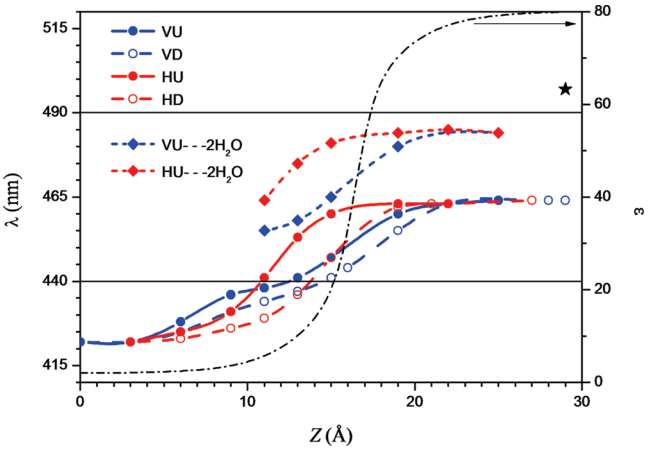


**Figure 8.** Fluorescence emission wavelengths (nm) calculated for conformer I of Acdan in the different alignments/orientations shown in Figure 5, as a function of the position of the center of the molecular frame across the lipid bilayer. Fluorescence emission wavelengths (nm) calculated for Acdan + 2 H-bonded waters in the alignments **V** and **H** with orientation **U** (Figure 5) are also reported. The star shows the wavelength in bulk water, as obtained by a QM/MM approach including polarization.[12] The horizontal lines indicate experimental values for Prodan and Laurdan in lipid bilayers.[4] The dashed−dotted line shows the profile of the position-dependent dielectric permittivity, $\varepsilon$, assumed in calculations. For symmetry reasons, only one-half of the bilayer is shown.

and characterized by a narrower distribution in the bilayer. As for Prodan and Acdan, even for Laurdan, the position distribution is predicted to slightly narrow and shift toward the bilayer surface upon going from the ground to the excited state due to the increase of exposed charges, which anchor the chromophore to the bilayer head group region.

L-shaped conformers of Laurdan are found to preferentially align the aromatic plane parallel to the acyl chains, with the long naphthalene axis perpendicular to the bilayer normal (**HU** orientation). In this way, they can direct the polar carbonyl group toward the hydrophilic region and bury the apolar tail in the hydrophobic core of the bilayer. As an example, we show in Figure 7 the orientational distribution calculated for the most stable of the conformers in its ground state, in the most probable position; a very similar plot was obtained for the excited state. More elongated conformers either align their long naphthyl axis roughly parallel to the bilayer normal (**VD** orientation), locating their carbonyl below the hydrophobic/hydrophilic interface, or tilt to bring it closer to the polar region of the bilayer. Because neither of these configurations optimizes electrostatic and anisotropic interactions at the same time, elongated conformers are found to be destabilized in the liquid-crystal phase of the bilayer.

Distributions similar to those shown in Figures 3 and 6, and analogous changes upon excitation, were recently reported from molecular dynamics simulations of Prodan and Laurdan in a liquid-crystalline DOPC bilayer;[57] there, no information was extracted on the orientational and conformational distribution of the probes, probably due to the long simulation times required for a meaningful sampling of these degrees of freedom.

**3.2. QM/PCM Fluorescence Profiles.** In this section, we report the fluorescence profiles obtained for Acdan using the QM/PCM approach described in section 2.1. The position of the probe was varied through the whole bilayer half-thickness,


dx.doi.org/10.1021/jp205163w |J. Phys. Chem. B 2011, 115, 9980–9989

while only few orientations of the chomophore were considered, shown in Figure 5, which were selected on the basis of the orientational distributions of the probes.

In Figure 8, we report (line−circles) the fluorescence emission wavelength calculated as a function of the position of the center of the molecular frame across the lipid bilayer. We can see that the emission is red-shifted by about 40 nm as the chromophore moves from the bilayer core to water and has some dependence on the probe orientation. At a given position, the emission wavelength increases as more charges reside in a polar environment, and for the same alignment, probes with the carbonyl group pointing toward water (**VU** and **HU**) are predicted to emit at a longer wavelength than those exposing the amino group (**VD** and **HD**).

For the preferred locations of the probes (see Figures 3 and 6), emission wavelengths in a range including the experimental blue-shifted emission, at about 440 nm,[4] are obtained. On the contrary, the red-shifted wavelength, experimentally observed near 490 nm, is even above that estimated for the probes in bulk water. To explain such findings, we have to recall that these results were obtained by a purely continuum model, which means that specific hydrogen-bonding effects are not explicitly included. In a recent study on solvatochromism of Prodan and other analogous probes,[12] some of us showed that in protic solvents, and in particular in water, the observed fluorescence wavelength is the result of a delicate combination of short-range (H-bonds) and long-range (polarity) solvent effects. By comparing different solvation models, it was shown that to obtain a good estimate of the fluorescence wavelengths in those solvents, a more refined approach has to be introduced by using extended QM/MM clusters. In Figure 8, the wavelength estimated for Prodan in bulk water by such a QM/MM approach including polarization[12] is also shown (star). An alternative strategy is to use smaller clusters of solvent molecules around the probe but include long-range effects with an external continuum dielectric. In the case of Prodan in water, we showed that at least two water molecules H-bonded to the carbonyl oxygen are required, the carbonyl group being the site involved in stronger H-bonds.[12]

The presence of H-bonds involving Prodan and water has been hypothesized also in lipid bilayers, at least when the carbonyl group resides in regions where water penetration is not negligible.[17,31,58] Therefore, we have repeated the QM/PCM calculations for the fluorescence profiles of Acdan H-bonded to two water molecules inside of the lipid bilayer. Both alignments **V** and **H** were considered, with orientation **U**, in which the CO group points outward. The emission wavelength profiles obtained in this way are reported in Figure 8 (line−diamonds). We can see that the presence of H-bonds yields a significant increase of the emission wavelength, leading the calculated values very close to the red-shifted experimental wavelength.

## 4. DISCUSSION

The results of the calculations reported and discussed in the previous section provide detailed insights into the distribution of the probes in lipid bilayers, both in the ground and in the excited state, which generally are not accessible by experiments because these report on suitably time- and space-averaged properties.

From the transfer free-energy profiles in Figures 3 and 6, the following ranking of affinity for the membrane is found, Laurdan > Prodan > Acdan, in agreement with the commonly accepted view, which is based on simple considerations on the hydrophobic character of the acyl chain and has been supported by experimental evidence in various conditions.[1,2,16,33]

The three probes are predicted to be inhomogeneously distributed across the bilayer. Preferential location of the naphthalene core in the glycerol region is in accord with the general belief for Prodan and Laurdan.[4,17,20,28,59,60] It is commonly stated that Prodan resides closer to the water/bilayer interface than Laurdan. This was inferred, with different motivations, from FTIR experiments at various pressures,[1,33] from steady-state and time-dependent fluorescence measurements,[5] and from parallax analysis of fluorescence quenching;[28] however, the ability of these experiments to unambiguously assess the probe position may be questionable. The weaker sensitivity of Laurdan to changes in the lipid head group region[32] and its stronger perturbing effect on the lipid chains,[33] if compared with those of Prodan, were ascribed to its deeper location in the bilayer. Actually, both may derive from the higher affinity of Laurdan for the hydrophobic region of the bilayer, determined by its longer acyl chain.[61]

A nonuniform distribution of the probes does not mean that these are anchored at a given site; they are rather predicted to span a range of positions, which may be as broad as 1 nm. This is probably a feature shared by most molecules with elongated shape, like Acdan and Prodan, inside of lipid bilayers; we obtained a similar result also for cholesterol,[39] in agreement with experimental findings.[62,63] Contributions from differently shaped conformers are responsible for further broadening of the distribution of Laurdan. The vertical heterogeneity is expected to modulate the interaction of probes with water and, therefore, their spectroscopic behavior, as determined in experiments of solvent relaxation,[5] generalized polarization,[3] and red edge excitation shift.[61]

Our calculations show the orientational and conformational preferences of the probes, which are generally ignored in the literature, where the representation of the chromophore in the "upright" orientation (**VD** in Figure 5) is adopted and the most extended "rod-like" conformation of Laurdan is assumed. For Acdan and Prodan, we have evidenced the existence of two preferential orientations, one parallel (or vertical, **V**) and the other perpendicular (or horizontal, **H**) to the bilayer normal; the former is promoted by the dispersion and anisotropic interactions in the apolar region of the bilayer, while the latter is favored by electrostatic interactions. As shown by the orientational distributions in Figure 4, a change from vertical to horizontal is predicted for the preferred orientation of Acdan and Prodan, along with relocation closer to the hydrophobic/hydrophilic interface, upon going from the ground to the excited state, as a consequence of the increased dipole. Even though the lifetime of fluorescence, on the order of nanoseconds, may not be sufficient for the probe to reach its equilibrium distribution in the excited state, this change may affect the emission spectra of Acdan and Prodan, as well as solvent relaxation. We expect the competition between preferential parallel and perpendicular orientations to be a general feature of polar dyes with elongated aromatic planes; one or the other orientation would dominate, depending on the state of the lipid bilayer and the polarity of the chromophore. Recent single-molecule fluorescence experiments for BODYP in DPPC supported bilayers evidenced the competition between the vertical and the horizontal orientation, prevailing under conditions of tight and loose lipid packing, respectively.[64,65] In the case of Laurdan, we predict horizontal orientation of the chromophore for L-shaped conformers, which are stabilized in

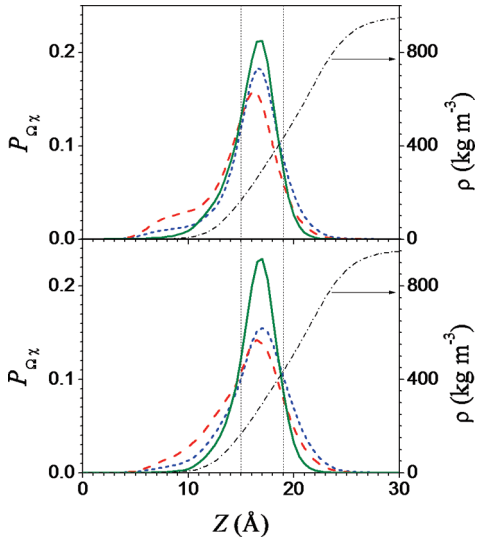


**Figure 9.** Position distribution $P_{\Omega,\chi}(Z)$ calculated for Acdan (blue short-dashed), Prodan (red dashed), and Laurdan (green solid) in the $S_0$ (top) and $S_1$ (bottom) states as a function of the position of the oxygen atom of their carbonyl group across a DPPC bilayer. The density profile of water[55] is shown for comparison (dashed−dotted line). The coordinate $Z = 0$ corresponds to the bilayer midplane; the vertical lines indicate the average position of carbonyl and phosphate groups of lipids. Given the symmetry of the system, only one-half of the bilayer is shown.

the liquid-crystal phase, and vertical alignment for elongated conformers. This result is compatible with experiments of two-photon excitation fluorescence microscopy, where circularly polarized light is used to excite probe molecules with the transition dipole (see Figure 2) on the focal plane.[20,66] In the equatorial region of vesicles, fluorescence was observed both in the liquid-crystal and in the gel phase, whereas emission in the polar region was only detected for the liquid-crystal phase (photoselection). Because it was assumed that in both phases the long naphthalene axis is preferentially oriented parallel to the bilayer normal, the lower degree of order in the liquid-crystal phase had to be invoked to explain this effect.[67] However if, as obtained by our calculations, a large amount of L-shaped conformers preferentially orient their transition dipole perpendicular to the bilayer normal in the liquid-crystal phase, emission from the polar region of vesicles is not surprising. We have not investigated the interaction of Laurdan with the bilayer in the gel phase, but a stabilization of elongated conformers, which preferentially align the chromophore axis to the bilayer normal, looks conceivable in this tightly packed environment. Thus, the differential emission in the gel and liquid-crystal phase would reflect a change in the conformational distribution of Laurdan and then in its orientational preference between the two phases.

The spectroscopic behavior of the fluorescent probes under investigation in lipid membranes is often described in terms of probe configurations more or less accessible to water; solutes embedded in the interior of the bilayer would be responsible for the emission at about 440 nm, close to that observed for the same probes in apolar isotropic solvents;[8−10] emission would be shifted at longer wavelengths for probes in the polar region. Our QM calculations have shown that hydrogen bonds with water molecules involving the carbonyl oxygen of the chromophore are needed to yield the large Stokes shifts corresponding to the emission observed at about 490 nm. Therefore, to discuss the fluorescence behavior of the three dyes, it is convenient to look at the distribution through the membrane of their carbonyl oxygen. The profiles, calculated as averages over all of the conformers and orientations, are shown in Figure 9, together with the density profile of water through a model liquid-crystalline DPPC bilayer.[55]

For all of the probes, the distribution of carbonyl oxygen spreads from the polar head group region, where water is abundant, to the apolar tail region, where the amount of water becomes negligible. Assuming that H-bonds are the major species responsible for the large Stokes shifts, their effects on the emission bands will increase with the water accessibility of the carbonyl oxygen.

The range of emission wavelengths due to probes in different positions and orientations can be discussed in light of the results of our QM calculations reported in Figure 8 (where the abscissa represents the position of the naphthalene center). The tails of the carbonyl distributions in Figure 9 correspond to probes in the upright orientation (**VD**), in which the carbonyl group is buried in the apolar region of the lipid tails; in the case of Laurdan, only the most extend conformers will contribute. These probes will not be involved in H-bonds, and their emission wavelength is predicted to span a range between 430 and 450 nm, in close agreement with the experimental reference value of 440 nm for the blue-shifted component of the emission spectrum. In the same range, also non-H-bonded chromophores in the **VU** and **HU** (and **HD** when significant) orientations, whose carbonyls are located below the hydrophobic/hydrophilic interface in Figure 9, are predicted to emit. H-bonded chromophores in the same orientations will emit at longer wavelengths, in the range between 455 and 465 nm for **VU** probes, and between 475 and 480 nm for **HU**/ **HD** probes, which is very close to the red-shifted component of the experimental emission spectrum, at about 490 nm. The not-perfect agreement between calculated and experimental data can be ascribed to some still-missing effects in the quantum mechanical simulation to be directly compared with the measured spectra, for example, vibronic effects are completely neglected. A similar underestimation was also obtained for Prodan in bulk water.[12]

The results of our calculations thus suggest a common origin of the features of the fluorescence spectra recorded in lipid membranes for the short- and long-tail probes. In the case of Laurdan, the positional heterogeneity of the carbonyl group is coupled to the conformational distribution; the carbonyl oxygen of L-shaped conformers would be more or less exposed to water, depending on the probe position, and then more or less involved in H-bonds, whereas that of elongated conformers would be buried in zones scarcely accessible to water. Elongated conformers, which are more ordered and are likely to reorient their transition dipole more slowly, might be responsible for the significantly higher steady-state fluorescence anisotropy observed at 440 nm than at 490 nm, a result which was not explained.[15] Somehow surprisingly, the role of molecular flexibility is generally disregarded when discussing the behavior of Laurdan in lipid bilayers. In fact, the acyl chain conformation is expected to have a scarce influence on the electronic transitions of Laurdan because these essentially involve the chromophore moiety. However, our results show that the chain conformation can affect the fluorescence emission in an indirect way by determining the location and orientation of the chromophore inside of the bilayer.

The relative weight of the long- and short-wavelength contributions in the emission spectrum will be affected by the physical state and the chemical composition of the bilayer, since temperature, pressure, the nature of lipid head groups, the length and unsaturation of acyl chains, and presence of perturbing agents influence the probe partition and water penetration in the bilayer. The stabilization of the elongated conformers of Laurdan in the gel phase, suggested by the two-photon excitation fluorescence microscopy experiments mentioned above,[66] is in agreement with the dominating blue emission observed in this condition.[4]

## 5. CONCLUSIONS

Polarity-sensitive fluorescence probes are an extremely useful tool for the investigation of lipid membranes because they can provide detailed information on the local structure, dynamics, and interactions. However, the need for a better understanding of the spectroscopic response has been pointed out in several instances;[57,58] this implies the connection between the electronic transitions of the probe and how these are affected by the environment, on one side, and the probe distribution in the bilayer and the factors that determine its changes as a function of bilayer composition or external perturbations, on the other side. The theoretical and computational techniques available nowadays seem to be mature to address this topic.

The integrated QM/PCM and MFT approach, which we have proposed here, appears suitable for a thorough analysis of the spectroscopic properties of fluorescent probes as a function of their interaction with the bilayer environment. The QM/PCM methodology reasonably accounts for the effect of the polarity of the heterogeneous environment on electronic transitions, and the MFT provides insights into the positional−orientational−conformational distribution of the probe, which is needed to predict spectroscopic observables.

The application of this integrated approach to the fluorescent probes Acdan, Prodan, and Laurdan in a model liquid-crystalline DPPC bilayer highlighted important effects. A strong dependence of the fluorescence emission wavelength on the position and orientation of the chromophore inside of the bilayer was evidenced by the QM/PCM calculations, and the molecular field analysis evidenced the actual role of different probe configurations in modulating the emission spectrum. In particular, nonobvious and usually disregarded effects of the orientational and conformational distributions of the probes emerged, which were shown to be able to indirectly affect the spectroscopic response. A complex picture is suggested, where the dynamic contributions, during the fluorescence lifetime, from probes heterogeneously distributed across the bilayer should be considered. The long-range electrostatic effects of the bilayer micropolarity were found to be insufficient to explain the origin of the red-shifted emission observed for Prodan and Laurdan in membranes; these could be accounted for by introducing the specific effects of H-bonding interactions between the probes and the water molecules penetrating into the bilayer. Thus, our analysis provides support to the hypothesis that the short- and long-wavelength maxima in the fluorescence spectra of Prodan and Laurdan correspond to a H-bond-free and a H-bonded form of the probe, respectively.[31]

Although, strictly speaking, our results refer to probes incorporated in a liquid-crystalline DPPC bilayer, some of our conclusions concerning the role of H-bonds and the importance of the conformational and orientational distribution of the probes are expected to be generally meaningful. However, due to the great sensitivity to the physical state and composition of the bilayer exhibited by the spectroscopic response, especially in the case of Prodan, the specific features of the lipid phase should be taken into account to get more accurate predictions, allowing a closer comparison with experiments.

The integrated approach used here for the first time appears suitable to bridge the spectroscopic behavior of polarity-sensitive probes and microenvironment properties of lipid membranes. It will be interesting to investigate other fluorescent probes; a further step will be the extension of our study to bilayers differing from liquid-crystalline DPPC in physical state and composition.

## ■ ASSOCIATED CONTENT

**Supporting Information.** Dipole moments of the probes, effect of different interactions on the transfer free energy of Acdan, orientational distribution of Acdan, and the definition of conformers of Laurdan and analysis of their individual contributions. This material is available free of charge via the Internet at http://pubs.acs.org.

## ■ AUTHOR INFORMATION

**Corresponding Author**

*E-mail: alberta.ferrarini@unipd.it (A.F.); bene@dcci.unipi.it (B.M.).

## ■ ACKNOWLEDGMENT

We acknowledge financial support from Università di Padova through PRAT-2009 (A.F.).

## ■ DEDICATION

This manuscript is dedicated to Alberto Marini, a friend and an enthusiastic scientist.

## ■ REFERENCES

(1) Chong, P.L.-G. *Biochemistry* **1988**, *27*, 399–404.
(2) Chong, P.L.-G. *High Pressure Res.* **1990**, *5*, 761–763.
(3) Parasassi, T.; De Stasio, G.; d'Ubaldo, A.; Gratton, E. *Biophys. J.* **1990**, *60*, 1179–1186.
(4) Parasassi, T.; Krasnowska, E. K.; Bagatolli, L.; Gratton, E. *J. Fluoresc.* **1998**, *8*, 365–373.
(5) Sỳkora, J.; Kapusta, P.; Fidler, V.; Hof, M. *Langmuir* **2002**, *18*, 571–574.
(6) Bagatolli, L. A. *Biochim. Biophys. Acta* **2006**, *1758*, 1541–1556.
(7) Lakowicz, J. R. *Principles of Fluorescence Spectroscopy*, 3rd ed.; Springer: Berlin, Germany, 2006.
(8) Weber, G.; Farris, F. J. *Biochemistry* **1979**, *1*, 3075–3078.
(9) Catalan, J.; Perez, P.; Laynez, J.; Blanco, F. G. *J. Fluoresc.* **1991**, *1*, 215–223.
(10) Cerezo, F. M.; Rocafort, S. C.; Sierra, P. S.; Garcia-Blanco, F.; Oliva, C. D.; Sierra, J. C. *Helv. Chim. Acta* **2001**, *84*, 3306–3312.
(11) Rowe, B. A.; Roach, C. A.; Lin, J.; Asiago, V.; Dmitrenko, O.; Neal, S. L. *J. Phys. Chem. A* **2008**, *112*, 13402–13412.
(12) Marini, A.; Munoz-Losa, A.; Biancardi, A.; Mennucci, B. *J. Phys Chem. B* **2010**, *114*, 17128–17135.
(13) Massey, J. B.; She, H. S.; Pownall, H. J. *Biochemistry* **1985**, *24*, 6973–6978.
(14) Vequi-Suplicy, C. C.; Benatti, C. R.; Lamy, M. T. *J. Fluoresc.* **2006**, *16*, 431–439.

(15) Lùcio, A. D.; Vequi-Suplicy, C. C.; Fernandez, R. M.; Lamy, M. T. *J. Fluoresc.* **2010**, *20*, 473–482.
(16) Zeng, J.; Chong, P.L.-G. *Biophys. J.* **1995**, *68*, 567–573.
(17) Kusube, M.; Matsuki, H.; Kaneshina, S. *Colloids Surf., B* **2005**, *42*, 79–88.
(18) Goto, M.; Sawaguchi, H.; Tamai, N.; Matsuki, H.; Kaneshina, S. *Langmuir* **2010**, *26*, 13377–13384.
(19) Zhang, Y.-L.; Frangos, J. H.; Chachisvilis, M. *Biochem. Biophys. Res. Commun.* **2006**, *347*, 838–841.
(20) Krasnowska, E. K.; Bagatolli, L. A.; Gratton, E.; Parasassi, T. *Biochim. Biophys. Acta* **2001**, *1511*, 330–340.
(21) Bondar, O. P.; Rowe, E. S. *Biophys. J.* **1999**, *76*, 956–962.
(22) Rottenberg, H. *Biochemistry* **1992**, *31*, 9473–9481.
(23) Parasassi, T.; Conti, F.; Gratton, E. *Cell. Mol. Biol.* **1986**, *32*, 99–102.
(24) Parasassi, T.; Conti, F.; Gratton, E. *Cell. Mol. Biol.* **1986**, *32*, 103–108.
(25) Sommer, A.; Paltauf, F.; Hermetter, A. *Biochemistry* **1990**, *29*, 11134–11140.
(26) Parasassi, T.; Gratton, E. *J. Fluoresc.* **1995**, *5*, 59–69.
(27) Sỳkora, J.; Hutterer, R.; Hof, M. In *Fluorescence Spectroscopy in Biology*; Hof, M.; Hutterer, R.; Fidler, V., Eds.; Springer Verlag: Berlin, Germany, 2005; p 71.
(28) Jurkiewicz, P.; Olzyńska, A.; Langner, M.; Hof, M. *Langmuir* **2006**, *22*, 8741–8749.
(29) Olzyǹska, A.; Jurkiewicz, P.; Hof, M. *J. Fluoresc.* **2008**, *18*, 925–928.
(30) Samanta, A.; Fessenden, R. W. *J. Phys. Chem.* **2000**, *104*, 8972–8975.
(31) Klymchenko, A. S.; Duportail, G.; Demchenko, A. P.; Mély, Y. *Biophys. J.* **2004**, *86*, 2929–2941.
(32) Parasassi, T.; De Stasio, G.; Ravagnan, G.; Rusch, R. M.; Gratton, E. *Biophys. J.* **1991**, *60*, 179–189.
(33) Chong, P.L.-G.; Wong, P. T. T. *Biochim. Biophys. Acta* **1993**, *1149*, 260–266.
(34) (a) Davis, B. N.; Abelt, C. J. *J. Phys. Chem. A* **2005**, *109*, 1295–1298. (b) Everett, R. K.; Nguyen, H. A. A.; Abelt, C. J. *J. Phys. Chem. A* **2010**, *114*, 4946–4950.
(35) (a) Ilich, P.; Prendergast, F. G. *J. Phys. Chem.* **1989**, *93*, 4441–4447. (b) Parusel, A. B. J.; Schneider, F. W.; Köhler, G. *J. Mol. Struct.: THEOCHEM* **1997**, *398*−*399*, 341. (c) Parusel, A. B. J.; Nowak, W.; Grimme, S.; Köhler, G. *J. Phys. Chem. A* **1998**, *102*, 7149–7156.
(36) Mennucci, B.; Caricato, M.; Ingrosso, F.; Cappelli, C.; Cammi, R.; Tomasi, J.; Scalmani, G.; Frisch, M. J. *J. Phys Chem. B* **2008**, *112*, 414–423.
(37) Tomasi, J.; Mennucci, B.; Cammi, R. *Chem. Rev.* **2005**, *105*, 2999–3093.
(38) (a) Frediani, L.; Cammi, R.; Corni, S.; Tomasi, J. *J. Chem. Phys.* **2004**, *120*, 3893–3907. (b) Frediani, L.; Mennucci, B.; Cammi, R. *J Phys. Chem. B* **2004**, *108*, 13796–13806. (c) Bondesson, L.; Frediani, L.; Ågren, H.; Mennucci, B. *J Phys. Chem. B* **2006**, *110*, 11361–11368.
(39) Parisio, G.; A. Ferrarini, A. *J. Chem. Theory Comput.* **2010**, *6*, 2267–2280.
(40) Stern, H. A.; Feller, S. E. *J. Chem. Phys.* **2004**, *118*, 3401–3412.
(41) Nagle, J. F.; Tristram-Nagle, S. *Biochim. Biophys. Acta* **2000**, *1469*, 159–195.
(42) Marsh, D. *Biochim. Biophys. Acta* **1996**, *1286*, 183–223.
(43) (a) Cancès, E.; Mennucci, B.; Tomasi, J. *J. Chem. Phys.* **1997**, *107*, 3032–3041. (b) Cancès, E.; Mennucci, B.; Tomasi, J. *J. Phys. Chem. B* **1997**, *101*, 10506–10517.
(44) Scalmani, G.; Frisch, M. J.; Mennucci, B.; Tomasi, J.; Cammi, R.; Barone, V. *J. Chem. Phys.* **2006**, *124*, 094107–15.
(45) Yanai, T.; Tew, D. P.; Handy, N. C. *Chem. Phys. Lett.* **2004**, *393*, 51–57.
(46) Caricato, M.; Mennucci, B.; Tomasi, J.; Ingrosso, F.; Cammi, R.; Corni, S.; Scalmani, G. *J. Chem. Phys.* **2006**, *124*, 124520–13.
(47) (a) Singh, U. C.; Kollman, P. A. *J. Comput. Chem.* **1984**, *5*, 129–145. (b) Besler, B. H.; Merz, K. M., Jr.; Kollman, P. A. *J. Comput. Chem.* **1990**, *11*, 431–439.
(48) Sanner, M. F.; Olson, A.; Spehner, J.-C. *Biopolymers* **1996**, *38*, 305–320.
(49) Cantor, R. S. *J. Phys. Chem. B* **1997**, *101*, 1723–1725.
(50) Gallicchio, E.; Levy, R. M. *J. Comput. Chem.* **2003**, *25*, 479–499.
(51) Tanizaki, S.; Feig, M. *J. Chem. Phys.* **2005**, *122*, 124706/1–124706/13.
(52) Ferrarini, A.; Moro, G. J.; Nordio, P. L.; Luckhurst, G. R. *Mol. Phys.* **1992**, *77*, 1–15.
(53) Flory, P. J. *Statistical Mechanics of Chain Molecules*; Interscience: New York, 1969.
(54) Ollila, O. H. S.; Róg, T.; Karttunen, M.; Vattulainen, I. *J. Struct. Biol.* **2007**, *159*, 311–323.
(55) Kupiainen, M.; Falck, E.; Ollila, S.; Niemelä, P.; Gurtovenko, A. A. *J. Comput. Theor. Nanosci.* **2005**, *2*, 401–413.
(56) Falck, E.; Patra, M.; Karttunen, M.; Hyvönen, M. T.; Vattulainen, I. *Biophys. J.* **2004**, *87*, 1076–1091.
(57) Barucha-Kraszewska, J.; Kraszewski, S.; Jurkiewicz, P.; Ramseyer, C.; Hof, M. *Biochim. Biophys. Acta* **2010**, *1798*, 1724–1734.
(58) Demchenko, A. P.; Mély, Y.; Duportail, G.; Klymchenko, A. S. *Biophys. J.* **2009**, *96*, 3461–3470.
(59) Antollini, S. S.; Barrantes, F. J. *Biochemistry* **1998**, *37*, 16653–16662.
(60) Bernik, D. L.; Zubiri, D.; Tymczyszyn, E.; Disalvo, E. A. *Langmuir* **2001**, *17*, 6438–6442.
(61) Krasnowska, E. K.; Gratton, E.; Parasassi, T. *Biophys. J.* **1998**, *74*, 1984–1993.
(62) Gliss, C.; Randel, O.; Casalta, H.; Sackmann, E.; Zorn, R.; Bayerl, T. *Biophys. J.* **1999**, *77*, 331–340.
(63) Harroun, T. A.; Katsaras, J.; Wassall, S. R. *Biochemistry* **2006**, *45*, 1227–1233.
(64) Livanek, P. W.; Huckabay, H. A.; Dunn, R. C. *J. Phys. Chem. B* **2009**, *113*, 10240–10248.
(65) Huckabay, H. A.; Dunn, R. C. *Langmuir* **2011**, *27*, 2658–2666.
(66) Bagatolli, L. A.; Gratton, E. *Biophys. J.* **2000**, *78*, 290–305.
(67) Bagatolli, L. A.; Gratton, E. *J. Fluoresc.* **2001**, *11*, 141–160.